Multiple Site Optical Recording of Transmembrane Voltage (MSORTV) in Patterned Growth Heart Cell Cultures: Assessing Electrical Behavior, with Microsecond Resolution, on a Cellular and Subcellular Scale

Stephan Rohr and B. M. Salzberg

Departments of Neuroscience and Physiology, University of Pennsylvania School of Medicine, Philadelphia, Pennsylvania 19104-6074, and Marine Biological Laboratory, Woods Hole, Massachussetts 02543 USA

ABSTRACT We have applied multiple site optical recording of transmembrane voltage (MSORTV) to patterned growth cultures of heart cells to analyze the effect of geometry per se on impulse propagation in excitable tissue, with cellular and subcellular resolution. Extensive dye screening led to the choice of di-8-ANEPPS as the most suitable voltage-sensitive dye for this application; it is internalized slowly and permits optical recording with signal-to-noise ratios as high as 40:1 (measured peak-to-peak) and average fractional fluorescence changes of 15% per 100 mV. Using a ×100 objective and a fast data acquisition system, we could resolve impulse propagation on a microscopic scale (15 μm) with high temporal resolution (uncertainty of ±5 μs). We could observe the decrease in conduction velocity of an impulse propagating along a narrow cell strand as it enters a region of abrupt expansion, and we could explain this phenomenon in terms of the micro-architecture of the tissue. In contrast with the elongated and aligned cells forming the narrow strands, the cells forming the expansions were aligned at random and presented 2.5 times as many cell-to-cell appositions per unit length. If the decrease in conduction velocity results entirely from this increased number of cell-to-cell boundaries per unit length, the mean activation delay introduced by each boundary can be estimated to be 70 μs. Using this novel experimental system, we could also demonstrate the electrical coupling of fibroblasts and endotheloid cells to myocytes in culture.

INTRODUCTION

The normal pump function of the heart depends upon the rapid and sequential activation of atria and ventricles. Determinations of the pattern of activation were undertaken as early as 1914 when Sir Thomas Lewis recorded the spread of excitation using a "roving" probe (Lewis et al., 1914). A complete picture of the activation of the heart was first given by Durrer et al. (1970), who determined the spatial pattern of excitation by employing multiple extracellular electrodes on human hearts. Since then, arrays of extracellular electrodes have provided the methodological background for a wide variety of investigations concerning normal as well as disturbed macroscopic impulse propagation (Wit et al., 1982; Ursell et al., 1985; Brugada et al., 1991; Pollard et al., 1993; Witkowski et al., 1994). Although this approach provided insights into a variety of mechanisms governing macroscopic impulse propagation, the low spatial resolution of the recording arrays rendered it incapable of yielding information concerning the dependence of microscopic impulse propagation on the structural arrangement of individual myocytes. This dependence was suggested, based on indirect evidence, more than a decade ago (Spach et al., 1981; Spach and Kootsey, 1983) but, in the absence of an appropriate experimental model, the possible influence of the discrete structure of cardiac tissue on propagation has been studied primarily by means of computer simulations (Rudy and Quan, 1987; Henriquez and Plonsey, 1987; Murphey et al., 1991a, b; Rudy and Quan, 1991; Shumaker et al., 1993). Only recently have there been attempts to increase the spatial resolution of extracellular arrays for mapping the spread of excitation at the single cell level in either cultures of myocytes (Israel et al., 1990) or in intact tissue (Spach et al., 1990).

Experiments designed to investigate the structure-function relationship between the cellular architecture of the excitable tissue and impulse propagation obviously must include the controlled variation of the structure of the network formed by individual myocytes, and should permit recording of the emerging patterns of electrical activity at high spatial (cellular/subcellular) and temporal resolution. The first condition was satisfied with the development of a method that allowed for precise geometrical patterning of the growth of myocytes in monolayer culture (Rohr et al., 1991). This system permits the design of 2-dimensional cell-networks having arbitrary geometry, and has the advantage that individual cells contributing to the function of the entire ensemble can be readily identified. In the present paper, we describe the application of a system for multiple site optical recording of transmembrane voltage (MSORTV) that meets the second condition, viz., the mapping of impulse propagation at high

Received for publication 1 March 1994 and in final form 13 May 1994.

Address reprint requests to Stephan Rohr, University of Bern, Department of Physiology, Bühlplatz 5, CH-3012 Bern, Switzerland. Tel.: 041-31-631-87-02; Fax: 041-31-631-46-11.

Dr. Rohr's present address: University of Bern, Department of Physiology, Bühlplatz 5, CH-3012 Bern, Switzerland.

Address correspondence to Brian M. Salzberg, Department of Neuroscience, University of Pennsylvania Medical School, 234 Stemmler Hall, Philadelphia, PA 19104-6074. Tel.: 215-898-2441; Fax: 215-573-2015; E-mail: salzberg@al.mscf.upenn.edu.

0006-3495/94/09/1301/15 $2.00

temporal and spatial resolution in these patterned cell ensembles. The MSORTV system is based on the use of potentiometric dyes (Cohen and Salzberg, 1978) that, although employed mainly in neurophysiology (Salzberg, 1983; Salzberg, 1989), have also found important application in cardiac electrophysiology (Salama and Morad, 1976; Morad and Salama, 1979; Sawanobori et al., 1981; Dillon and Morad, 1981; Windisch et al., 1985; Rosenbaum et al., 1991; Loew et al., 1992; Pertsov et al., 1993; Witkowski et al., 1994; for review, see Kamino, 1991). The optical determination of electrical activity in thin preparations by means of voltage sensitive dyes has several advantages over the use of extracellular electrodes: (i) it reports transmembrane voltage changes originating exclusively from the region imaged by a single photodetector in an array, permitting a precise spatially resolved picture of voltage fluctuations; (ii) the spatial resolution of this technique is theoretically limited only by the optical magnification, the size of each photodetector, and signal-to-noise considerations; (iii) because *transmembrane* voltage changes are monitored, optical recordings provide clearly defined reference parameters (e.g., dV/dt max. or the time of 50% depolarization) with which microscopic activation maps can be constructed; (iv) the optical approach is extremely flexible, permitting one to switch rapidly to any location of interest in a preparation, or to increase/decrease the spatial resolution according to the objectives of a specific experiment. Disadvantages compared with extracellular electrodes include phototoxic effects resulting from free radical production by the excited states of the dyes, which can limit recording times.

The present paper describes the development of a fluorescence measurement technique suitable for monolayer cultures of cardiac myocytes with the aim of recording electrical activity with variable spatial resolution from the multicellular to the subcellular scale. We will discuss the measures required to optimize the staining and illumination conditions, and we will detail the limits of the method in terms of phototoxic effects. Finally, we will present data that suggest that impulse propagation in cultures of cardiac myocytes is dependent on the packing arrangement of the cells, and we will show that myocytes are electrically coupled to nonmyocytes of cardiac origin, i.e., to fibroblasts and endotheloid cells. Part of this work has previously been published in abstract form (Rohr and Salzberg, 1992a).

MATERIALS AND METHODS

Cell cultures

Cultures were established according to a slightly modified conventional technique (Rohr et al., 1991). Briefly, 8–10 neonatal rats (Sprague-Dawley, Charles River Laboratories) were anesthetized with ether (Fisher Scientific, Pittsburgh, PA), and the hearts were quickly removed and placed in ice-cold Hank's balanced salt solution lacking Ca^{2+} and Mg^{2+} (Gibco BRL, Grand Island, NY). The lower two-thirds of the ventricles were minced into pieces approximately 1 mm on a side, and were transferred to a dissociation solution consisting of Hank's balanced salt solution, again lacking Ca^{2+} and Mg^{2+}, 0.1% trypsin (Boehringer, Indianapolis, IN), 60 μg/ml pancreatin (Sigma Chemical Co., St. Louis, MO), 20 μg/ml streptomycin, and 20 units/ml penicillin (Fakola, Basel, Switzerland). This suspension was gently stirred at 35°C for 15 min and, after settling of the tissue fragments, the supernatant of the first dissociation was discarded and stirring was resumed after addition of fresh dissociation solution. This cycle was repeated until the tissue fragments were fully dissociated (3–4 cycles). The supernatant cell suspensions of each of these subsequent dissociation cycles were collected, temporarily stored on ice, and finally centrifuged. The resulting cell pellets were resuspended in culture medium, combined and filtered through a cotton mesh (Flawa AG, Flawil, Switzerland). The culture medium consisted of M199 with Hank's salts (Gibco BRL), 10% newborn calf serum (Hyclone, Logan, UT), 1.5 μM vitamin B12 (Sigma), 20 μg/ml streptomycin, and 20 units/ml penicillin (Fakola). The resulting cell suspension was transferred to cell culture flasks (Gibco BRL) and was preincubated for 2 h in an incubator at 35°C in a water-saturated atmosphere of ambient air and 1.4% CO_2 to remove fibroblasts and endotheloid cells (Hyde et al., 1969). Thereafter, the cell density was determined with a hemocytometer and cells were plated at 2000 cells/mm^2. Medium exchanges were performed every other day with culture medium containing 5% newborn calf serum. Patterned growth was obtained by plating the cells onto #0 coverslips precoated with patterns of a light-sensitive resin (photoresist) that rejected adhesion of cells (Rohr et al., 1991).

Experimental protocol

The cover slips with adherent cell cultures were transferred to a temperature-controlled superfusion chamber (Rohr, 1986) and were mounted on the microscope stage. Because objectives with short working distances and high numerical apertures were used, the chamber was slightly modified so that the thin coverslips themselves formed its bottom. The preparations were superfused by means of a Holter peristaltic pump (Critikon Corp., Tampa, FL) at 5–10 ml/min with Hanks' balanced salt solution (Gibco BRL) containing (mM) NaCl 137, KCl 5.4, $CaCl_2$ 1.3, $MgSO_4$ 0.8, $NaHCO_3$ 4.2, KH_2PO_4 0.5, Na_2HPO_4 0.3, and Na-HEPES 10 (adjusted to pH 7.35 with HCl). All experiments were carried out at 35°C. The screening of the dyes was performed with spontaneously contracting cultures exhibiting beat rates ranging between 50 and 150 beats/min. In a few additional experiments, the cultures were stimulated at a point with extracellular glass electrodes (Corning, tip diameter 3–5 μm) that were filled with a 3 M KCl-Agar solution and were attached to micromanipulators (Narishige Scientific Instrument Laboratory, Tokyo, Japan; Zeiss MR-3 Mot, Carl Zeiss Inc., Thornwood, NY). Impulses were generated by a stimulator (Grass Instrument Co., Quincy, MA) delivering square pulses of 1-ms duration at twice threshold intensity. Stimulation electrode(s) were positioned at least 1–2 mm from the optical recording site. This distance corresponds to 3–6 times the space constant determined earlier in a similar culture system (360 μm; Jongsma and van Rijn, 1972) and only permitted propagated action potentials to invade the region under investigation. Then, superfusion was halted and the preparations were stained with 2 ml of a solution of voltage-sensitive dyes (c.f. below) for 3–5 min. After staining, the preparations were washed, superfusion was resumed, and experiments were begun after an equilibration period of 5–10 min. Conventional intracellular recordings were obtained using glass microelectrodes filled with 3 M KCl (tip resistance around 10 MOhm) that were mounted on a micromanipulator and were connected to an electrometer amplifier (Axoprobe 1A, Axon Instruments Inc., Foster City, CA).

Dyes

Applying optical recording methods to heart cells in culture for the first time forced us to screen a variety of absorption as well as fluorescent dyes. Among the absorption dyes, we evaluated NK 3041 (=RH155; Grinvald et al., 1980), NK2761 (Kamino et al., 1981; Salzberg et al., 1983), NK2367 (Salzberg et al., 1977), WW781 (Ross et al., 1977; Morad and Salama, 1979; Witkowski et al., 1994), and RH472. All of the fluorescent dyes tested belonged to the class of fast potentiometric dyes of the styryl type: di-4-ANEPPS, di-8-ANEPPS, di-12-ANEPPS (kindly supplied by Dr. Leslie Loew), RH 160, RH 237, RH 246, RH 418, RH 421, RH 423, RH 1385, RH

1405, RH 1413, RH 1419, RH 1422, and RH 1425 (kindly supplied by Dr. Amiram Grinvald and Rina Hildesheim). Some of these dyes are now available from Molecular Probes (Eugene, OR). Stock solutions (2–8 mg/ml) were prepared either by dissolving the dyes in ethanol or in a mixture of 75% w/w DMSO (Chempure brand; Curtin Matheson Scientific Inc., Houston, TX) and 25% w/w Pluronic F127 (BASF, Wyandotte, MI). In a few cases, the dyes were dissolved in a solvent consisting of a 1:1 (v/v) mixture of these two stock solvents. The stock solutions were tightly capped and stored in a freezer. Fresh staining solutions were prepared immediately before the experiments by adding appropriate amounts of the gently warmed stock solution to Hanks' balanced salt solution. The concentration of the stock solvent in the final staining solution was generally 0.5% and never exceeded 1%. The finding that the values determined optically for the upstroke and conduction velocity were within the range of values obtained during earlier microelectrode studies (Rohr et al., 1991) suggests that neither the dye nor its "vehicle" had any adverse effects on these electrophysiological parameters.

Multiple site optical recording of transmembrane voltage (MSORTV)

An overview of the measurement apparatus is given in Fig. 1. The apparatus was built around an inverted microscope (IM35, Zeiss, Oberkochen, Germany), equipped for epifluorescence, and attached to a large micrometer-driven X-Y positioner (Parsons et al., 1991) mounted on a vibration isolation table (Newport Corp., Irvine, CA). The light from a tungsten halogen lamp (250 W, Osram AG, Munich, Germany) or from a xenon short arc lamp (150 W, Osram; lamphousing 770 UW/T and D.C. power supply 1600 from Optiquip, Highland Mills, NY) was band-limited by interference filters (Omega Optics, Inc., Brattleboro, VT) and deflected towards the objective by means of a dichroic mirror (Omega Optics Inc., Brattleboro, VT). Longer wavelength fluorescence emission from the preparation passed through the dichroic mirror and a barrier filter (OG or RG glass; Schott Optical Glass Co., Duryea, PA) that blocked the scattered excitation light. The excitation filters were generally bandpass interference filters, and their specifications will be expressed as CWL(FWHM) throughout this paper (CWL: center wavelength (nm); FWHM: full width at half maximum transmission (nm)). Shortpass interference filters will be denoted as <WL (WL: cutoff wavelength (nm)), and long pass filters, which were generally Schott glass, will be denoted as >WL (WL: 50% transmission wavelength (nm)).

The image of the preparation was projected onto a 12 × 12 array of silicon photodiodes (MD-144-0, Centronics, Newbury Park, CA; *inset* "PDA" in Fig. 1). The individual square pixels of the array were 1.4 mm on a side and were separated by 0.1 mm. The pixel area corresponded to receptive fields in the object plane of 60 μm × 60 μm (×25 objective), 22 μm × 22 μm (×63 objective), and 15 μm × 15 μm (×100 objective). The photocurrents generated by the central 124 detectors were converted to voltages by first-stage amplifiers having 10^9 ohm feedback resistors, and were further amplified by an AC-coupled second-stage (AC coupling time constant of 3 s) having a gain of 50, resulting in an overall gain 5×10^{10} V/A (electronics shop, Yale University School of Medicine, Department of Physiology, New Haven, CT). Resting fluorescence was measured in a DC-coupled mode, with the second stage at unity gain. The noise was detector- and amplifier-limited and was typically 0.6 pA RMS referred to the input.

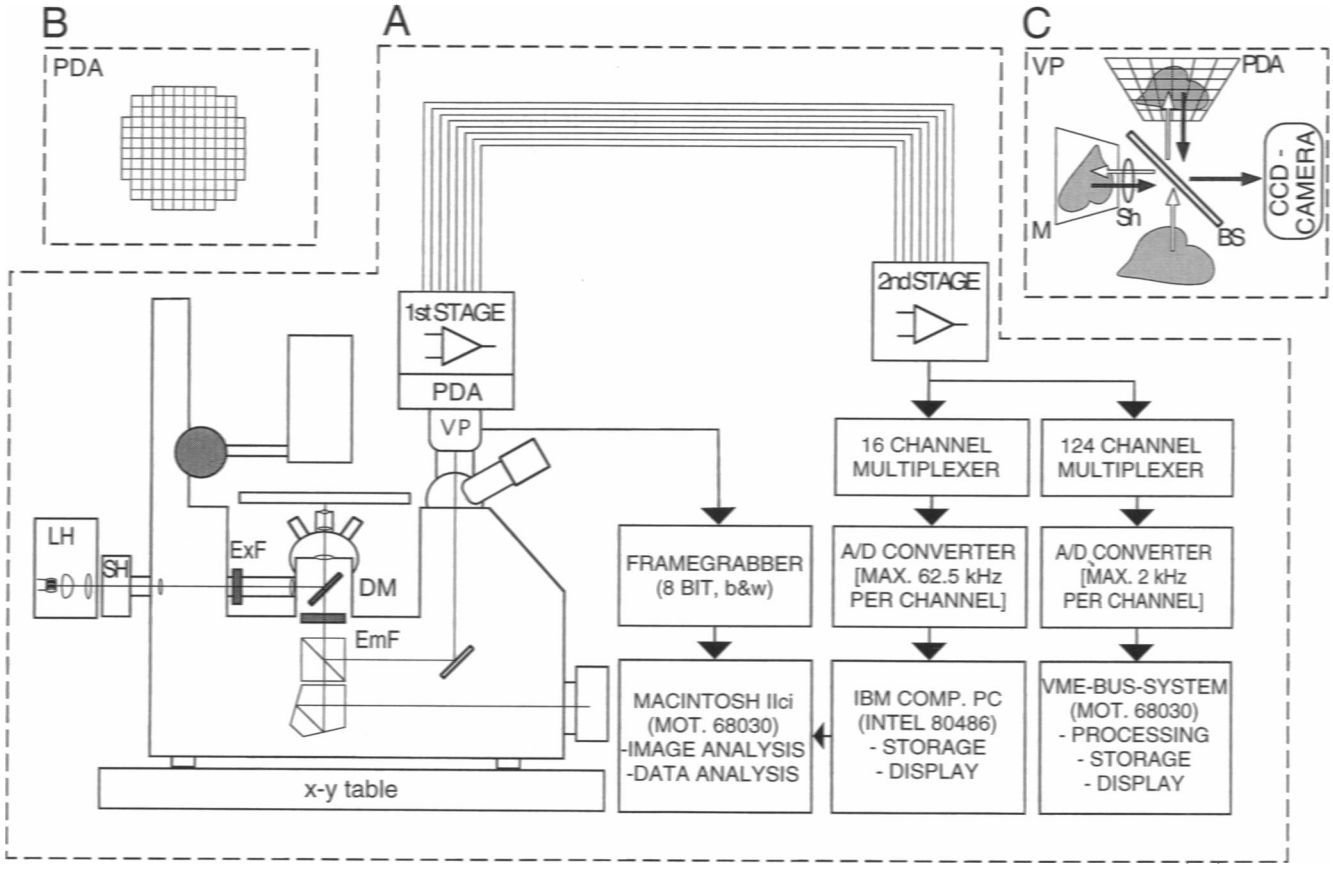

FIGURE 1 Schematic drawing of MSORTV system. (*A*) Overview of the components of the complete recording system, for details c.f. Materials and Methods. Abbreviations: light housing (LH), shutter (SH), excitation filter (ExF), dichroic mirror (DM), emission filter (EmF), video port (VP), photodiode-array (PDA). (*B*) Spatial arrangement of the 124 individual photodetectors composing the photodiode-array. Each square represents a single photodetector. (*C*) Schematic drawing of the imaging beamsplitter (VP). Components: 50% beamsplitter (BS), photodiode-array (PDA), mirror (M), shutter (SH); for details, see Materials and Methods.

The response time constant of each amplifier pair was individually fine-tuned to achieve a uniform temporal response among all amplifiers. The RC time constant chosen was 300 μs (3-dB point at 530 Hz), and the range of deviations from this mean value after tuning was ±15 μs. To increase the homogeneity of response times even further, the temporal deviations among the subset of amplifiers sampled at high speed (see below) were assessed at the beginning and at the end of each experimental series by means of a square light pulse from a light-emitting-diode (LED). The mean temporal differences between 40 and 60% increase in light current among all amplifiers during this LED-pulse were determined in increments of 2%, and the average was used to correct the timing of the original signals. This procedure further reduced the variability in response times among the amplifier pairs to less than ±5 μs.

The signals from all 124 diodes were multiplexed, digitized (maximum rate of 2000 frames per s), and stored in a computer (VME-bus Motorola 68030 operating under Versados). Analog outputs from an arbitrarily selectable subset of up to 16 channels were routed in parallel to a fast PC-based data acquisition system (Northgate 486i, Northgate Computer Systems, Minneapolis, MN equipped with a Flash-12 model 1 data acquisition card from Strawberry Tree Inc., Sunnyvale, CA). This data acquisition system was capable of acquiring 1 million samples (12 bit) at variable conversion rates up to 1 MHz. During the simultaneous data acquisition from 16 channels, the maximal conversion rate per channel was 62.5 kHz. Because the switching rate among the channels was fixed at 1 μs, the delay between the first and the last scanned channel was always fixed at 16 μs even at slower than maximal conversion rates (burst sampling). This delay was partially corrected for by the timing correction routine described above. Data acquisition rates were chosen according to the objectives of the experiments and varied between 5 and 62.5 kHz.

The analysis of the acquired data was performed on a second PC (Macintosh IIci, Apple Inc., Cupertino, CA) using routines developed in a spreadsheet program (Excel, Microsoft Corporation, Redmond, WA). Data were compensated for their offset and normalized for comparison purposes. To remove occasional spikes (most probably because of glitches occurring in the analog-to-digital conversion process occurring as single events in ~1% of the recordings), data were passed through a median filter encompassing five consecutive values. This filter substituted outlying values by their closest neighbors without affecting the rest of the data and, in particular, had negligible impact on the rapidly rising upstroke of the optically recorded action potential.

Activation delays between recording sites of interest were determined as the average of the differences in activation times at 11 evenly spaced intervals between 40 and 60% of full action potential amplitude at each site. Activation times at these discrete depolarization levels were obtained using linear interpolation between nearest actually measured values (at least 6 in the 40–60% depolarization range at an upstroke velocity of 200 V/s and a sampling rate of 62.5 kHz).

The maximal slope of the fast positive deflection of the optical signal was determined from the slope between adjacent measurement points. Because the presence of noise sometimes introduced false high slope values, characterized as sudden jumps in the slope versus time graph, we also filtered the data with a running average over three values. This procedure tended to lower slightly the slope of data acquired at low conversion rates without affecting, however, calculated activation delay times between individual detectors. To express slope values in familiar units, we assumed, based on previous measurements (Rohr et al., 1991) the action potential amplitude to be 100 mV and expressed the slope in V/s accordingly. In general, this procedure resulted in optically recorded upstroke velocities that fell within the range of those obtained previously using conventional microelectrode impalements in patterned growth heart cells (70–200 V/s; Rohr et al., 1991).

High resolution images of the myocyte cultures were recorded with either a 35-mm camera attached to the microscope (Contax 167 MP, Yashica Inc., Somerset, NJ) or with a CCD camera (Sony XC-77, Sony Corp., Paramus, NJ) attached to the side port of a beam-splitting cube that was inserted into the light path of the microscope in front of the photodetector array. This arrangement is depicted schematically in inset "VP" in Fig. 1. After passing the beam-splitting cube (50% transmission:50% reflection; Carl Zeiss Inc.), the projecting rays from the microscope were partially reflected from the photodiode array and, after a further reflection by the beam splitting cube, passed a zoom-lens system and were imaged by the CCD camera. Because the 0.1 mm wide boundary regions between the photodiode array elements are less reflective than the silicon diodes themselves, the preparations imaged with the CCD sensor carried a faint but distinct grid pattern that corresponded to the lines separating individual diodes. This permitted the precise localization of the "receptive fields" of individual diodes in the object plane. To enhance the brightness of the images in cases of faintly stained preparations, a front-surface mirror was attached at right angles to the beam splitting cube and equidistant from the photodiode array. The position of this mirror was carefully adjusted to obtain a perfect registration of the images reflected by the mirror and by the photodiode-array. By opening a shutter in front of the mirror, the brightness of the reflected image from the photodiode-array was enhanced by the overlaid secondary image from the mirror. However, because of the higher reflectivity of the mirror compared with that of the photodiode-array, this brightness enhancement was often accompanied by a loss of the grid lines. In these cases, we recorded two images, one with and one without brightness enhancement, respectively. Alternatively, a videomicrograph of the surface structure of the array alone was acquired at the beginning and, for control purposes, at the end of an experimental series, and the grid pattern corresponding to the detector array was digitally overlaid on the images of the preparations.

The CCD camera was normally operated in automatic gain control mode. A fixed gain was chosen during the course of photometric experiments. Images from the CCD camera were recorded using a computer-based image acquisition system connected to the video camera (Apple Macintosh IIci, equipped with a framegrabber, Quickcapture, Data Translation Inc., Marlboro, MA; image analysis software "Image," NIH, Bethesda, MD).

RESULTS

Dye selection: fractional fluorescence changes and signal-to-noise considerations

The ideal potentiometric probe for a specific application is a very sensitive transducer of changes in transmembrane potential and has little or no tendency to harm the preparation as the result of pharmacological or phototoxic side effects. Because these properties generally vary for a specific dye depending upon the preparation used (Waggoner and Grinvald, 1977; Cohen and Salzberg, 1978; Salzberg, 1983; Grinvald et al., 1988), it was necessary to screen a variety of dyes for their suitability for this particular application. Preliminary experiments were carried out with the absorbance dyes NK 2761, NK 2367, WW 781, RH 155, and RH 472 without obtaining any useful optical signal related to transmembrane voltage changes. However, most of the fluorescent dyes tested (di-4-ANEPPS, di-8-ANEPPS, RH 160, RH 237, RH 246, RH 421, RH 423, RH 1385, RH 1405, RH 1413, RH 1419), all of which belong to the class of fast styryl dyes, behaved as more or less successful transducers of transmembrane voltage changes. Not surprisingly, dyes that stained the cell membranes intensely, resulting in a bright enhancement of the cell borders, were also the dyes that gave the best optical signals (Grinvald et al., 1982; Chien and Pine, 1991). The sensitivity of the dyes for detecting transmembrane voltage changes was assessed by measuring the fractional change in fluorescence ($\Delta F/F$) in response to spontaneous action potentials generated in myocyte monolayers, and the data for the most sensitive dyes are summarized in Table 1. Fluorescence was excited with a tungsten halogen lamp, and the preparations were imaged with a ×63 (1.4 N.A.) oil immersion objective (Zeiss Planapo). The values

TABLE 1 Fractional fluorescence change per action potential amplitude (~100 mV)

Staining			Illumination			Fractional change		
Dye	Stock solvent	Staining conc. (μg/ml)	Excitation bandpass (nm)	Dichroic mirror (nm)	Emission (longpass) (nm)	$\Delta F/F$ (%) (per ~100 mV) mean ± SE	$\Delta F/F$ max. (%)	n
di-8-ANEPPS	DMSO/F127	40	520(90)	580	>590	10.3 ± 1.8	12.3	4
di-4-ANEPPS	EtOH/DMSO/F127	40	540(60)	580	>590	6.8 ± 2.7	10.8	6
RH 423	EtOH	20	520(90)	600	>610	8.5 ± 2.7	12.0	4
RH 421	EtOH	20	520(90)	600	>610	4.4 ± 0.3	4.8	3
RH 160	EtOH	5	520(90)	600	>610	2.5 ± 0.4	3.1	5

Specifications for excitation filter: wavelength of bandpass filter (FWHM = full width at half-maximum transmission).

represent the average of the $\Delta F/F$-maxima obtained in n determinations with 16 measurement sites each, and the percentage change can be referred to a transmembrane voltage change of approximately 100 mV, the typical amplitude of action potentials in this culture system (Rohr et al., 1991). Although all of the dyes exhibited good voltage sensitivity, RH 423 with a maximal fractional fluorescence change of 12.0% and di-8-ANEPPS with 12.3% were the most effective optical transducers of membrane potential. Because the optical filters were selected to maximize the absolute signal amplitude and, thereby, the signal-to-noise ratio, the values of $\Delta F/F$ reported could have been improved, at the expense of the signal-to-noise ratio, by using narrower bandwidth excitation and emission filters. This was verified in later experiments where, using the brighter 150 W xenon short arc lamp, excitation bandwidths could be narrowed to 50 nm (FWHM) and average $\Delta F/F$ ratios measured in preparations stained with di-8-ANEPPS ranged between 15 and 18%. The highest fractional fluorescence change per action potential ever observed reached 22.3%, and was measured in a monolayer stained with 80 μg/ml di-8-ANEPPS (excitation: 530(50) nm; dichroic mirror: 600 nm; emission filter: RG610).

To determine the direction and velocity of individual propagating impulses at the cellular level, it was imperative that the signal-to-noise ratio be large enough to record essentially undisturbed action potential upstrokes during single shot experiments, from which reliable activation delays could be determined. The signal-to-noise ratio is proportional to the fractional fluorescence change for a given transmembrane voltage change, and is proportional to the amount of total fluorescence if the measurements are, as was the case in our apparatus, limited by the noise (3.6 pA peak-to-peak) arising from the photodetector-amplifier combination. After identifying the dye exhibiting the highest $\Delta F/F$ ratio, we attempted to increase the overall fluorescence. This was achieved by (i) using relatively wide-band excitation filters and by (ii) introducing a brighter illumination source. Although wider-band excitation caused a decrease in $\Delta F/F$, the resulting increase in total signal size more than compensated for this effect. For example, replacement of the 530(50) excitation filter by a filter with a wider bandwidth (530(70)) resulted in a decrease in the mean $\Delta F/F$ from 18%/100 mV (n = 9) to 9%/100 mV (n = 3), whereas the signal-to-noise ratio, referred to the action potential amplitude (peak-to-peak), increased from 6.5 to 10.1 (dichroic mirror and emission filter unchanged at 600 nm and >610 nm, respectively; preparations stained with 80 μg/ml di-8-ANEPPS). Signal-to-noise ratios achieved with this regimen generally ranged from 7 to 12 (peak-to-peak). The ratio was trebled with the exchange of the tungsten halogen lamp for a 150 W xenon short arc lamp; under comparable staining conditions, this led to an increase in average resting fluorescence from 0.3 to 1 nA (expressed as diode photocurrents). With this arrangement, signal-to-noise ratios for action potentials in single shot experiments ranged between 25 and 40, corresponding to noise in the transmembrane voltage in the range of 2.5–4 mV.

Dye selection: bleaching and phototoxicity

The duration of an experiment with voltage-sensitive dyes is typically limited either by bleaching of the probe molecules leading to a decline in the signal-to-noise ratio, or by phototoxic effects attributable to free radical products, particularly singlet oxygen, of the excited state of the dye molecules (Oxford et al., 1977; Salzberg, 1983). Because we were interested in carrying out experiments requiring continuous illumination for more than 10 s, we reevaluated the four best dyes emerging from the previous tests with respect to photostability and freedom from phototoxicity. For this purpose, spontaneously active myocyte monolayers were stained with di-8-ANEPPS, di-4-ANEPPS, RH 421, or RH 423 at 20 μg/ml each. After equilibration, the preparations were monitored continuously for up to 60 s, and the time constant of the decay of the optical signal amplitude was determined. The results of these experiments are shown in Fig. 2. The average time constant measured with di-8-ANEPPS (24 s) was more than twice as long as that measured with any of the other three dyes. Because the decay of the signal amplitude could have been caused either by bleaching of the dye molecules or by an actual decrease in action potential amplitude resulting from phototoxic effects, we compared the time-course of bleaching alone (amplifiers DC-coupled) with that of the decay of the signal amplitude for the case of di-8-ANEPPS and di-4-ANEPPS during continuous illumination of up to 60 s. The results of these experiments are illustrated

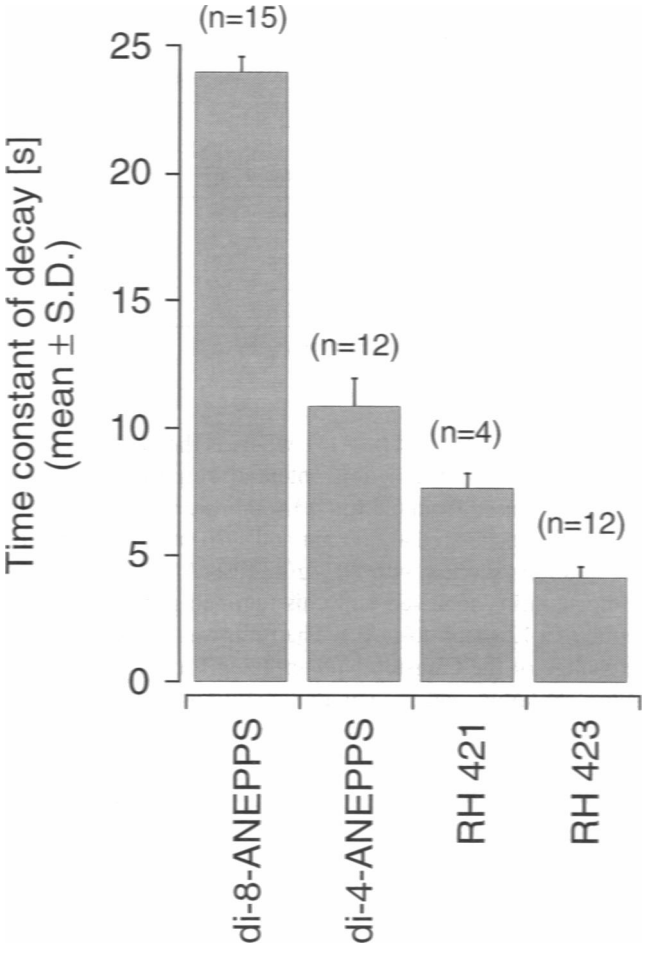

FIGURE 2 Time constant for decay of the signal amplitude for four different styryl dyes. Each column indicates, for a particular dye, the average time constant obtained from *n* determinations of the decay of the optical signal amplitude during continuous illumination.

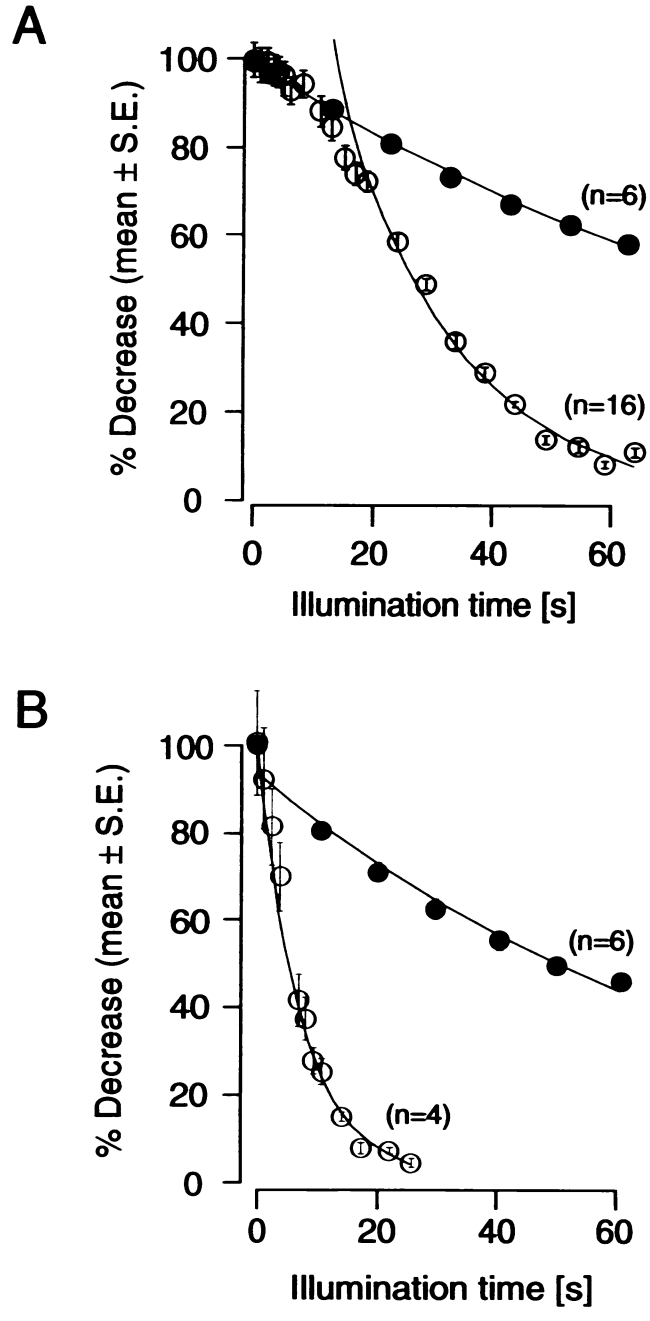

FIGURE 3 Comparison between the time course of dye bleaching and the time course of the decay of the signal amplitude during continuous illumination. Normalized decay of signal amplitude (○) and decrease in total fluorescence (●) for di-8-ANEPPS (*A*) and di-4-ANEPPS (*B*). The data are fitted with single exponentials.

in Fig. 3. For both dyes, the timecourse of the bleaching could be fitted with a single exponential ($R = 1.0$ and 0.99 for di-8-ANEPPS and di-4-ANEPPS, respectively) with di-8-ANEPPS showing slightly greater photostability. The major difference between the two dyes, however, was found in the time course of the decay of the signal amplitude. In the case of di-4-ANEPPS, the timecourse could be fitted with a single exponential ($R = 0.99$) with a decay rate roughly 10 times faster than that of bleaching alone. In the case of di-8-ANEPPS, however, the exponential decay of the signal amplitude started only after 18 s of continuous illumination, and with a decay rate "only" 6 times faster than that of bleaching alone. During the initial 18 s of illumination, the evolution of the di-8-ANEPPS signal amplitude first matched the bleaching curve before the decay rate began to accelerate, finally joining the exponential decrease. On the assumption that the bleaching process of the dye molecules located in the cell membrane and of the dye molecules internalized into the cytoplasm (cf. below) is identical, it is possible to suppose that any deviation of the timecourse of the decay of the signal amplitude from that of bleaching alone is the result of a true decrease in action potential amplitude and can serve, therefore, as an index of the severity of the phototoxic effects produced by the dyes concerned. Di-8-ANEPPS seemed to offer a window lasting more than 10 s, during which phototoxic effects were mostly absent, whereas di-4-ANEPPS started to affect the viability of the preparation from the very onset of illumination.

Transfer of dyes into the cytoplasm

Having examined the two dyes under identical conditions, the natural explanation for this difference in phototoxicity

was the slightly different molecular structure of the two compounds. Although the length of the double alkyl chains bonded to the aniline nitrogen is 8 carbon atoms in the case of di-8-ANEPPS, it is only 4 carbon atoms in the case of di-4-ANEPPS. This difference renders di-8-ANEPPS more hydrophobic and, by analogy with other dyes, it is likely that its anchoring in the cell membrane is more stable than that of di-4-ANEPPS (Fluhler et al., 1985). Indeed, we made the observation that di-4-ANEPPS leaked more easily into the interior of cells than did di-8-ANEPPS. The internalization of the dye was discernible through the increasing staining of intracellular organelles with time. This intracellular staining which, regardless of the type of dyes used, always occurred to a variable degree after successful staining of the membrane, led to the formation of bright rings around the nucleus and bright, randomly distributed granules in the cytoplasm. In contrast with the perinuclear increase in fluorescence, the amount of fluorescent staining in the center region of the nucleus remained unchanged because the nucleus, being devoid of intranuclear membranous structures, offered little or no binding substrate for the dyes which, even if they were present in the nucleoplasm, remained in an aqueous environment and, thus, were virtually nonfluorescent. Panels *A* and *B* of Fig. 4 illustrate this finding. The preparations had been stained with 80 μg/ml di-8-ANEPPS, and panel *A* is a videomicrograph showing the fluorescence immediately after staining. The contours of the cells were enhanced by bright staining of the cell membrane, whereas the nucleus was not discernible. However, 38 min after staining, the intense membrane staining had decreased, whereas the nuclei became prominent as a result of an acquired bright perinuclear halo. Based on this finding, we used the ratio of perinuclear to nuclear fluorescence as an indicator of the degree of internalization of individual dyes (ratio = 1, indicating no increase in intracellular staining). We determined the evolution of the brightness at different locations in the preparation photometrically using images acquired with the CCD camera (automatic gain control off) connected to a framegrabber having 8-bit resolution (256 gray levels). Nuclear and perinuclear brightness values were obtained from intensity profiles constructed across the center of the nuclei and were corrected for background light levels. Measurements were carried out at regular intervals up to 1 h after staining, and the results obtained with di-4-ANEPPS and di-8-ANEPPS are shown in panel *C* of Fig. 4. Less than 10 min after staining, the increase in perinuclear fluorescence had, in the case of di-4-ANEPPS, already reached more than 50% of the steady-state value attained 30 min after the beginning of staining. In contrast, di-8-ANEPPS resulted in negligible intracellular staining during the first 10 min after washing away the bath applied dye and reached values comparable with those seen in the case of di-4-ANEPPS only after a gradual increase in intracellular fluorescence over 40 min. This finding is consistent with the idea that dyes with longer alkyl chains are better retained in the cell membrane and, therefore, permit recording of transmembrane voltage changes for longer durations than do their short alkyl chain

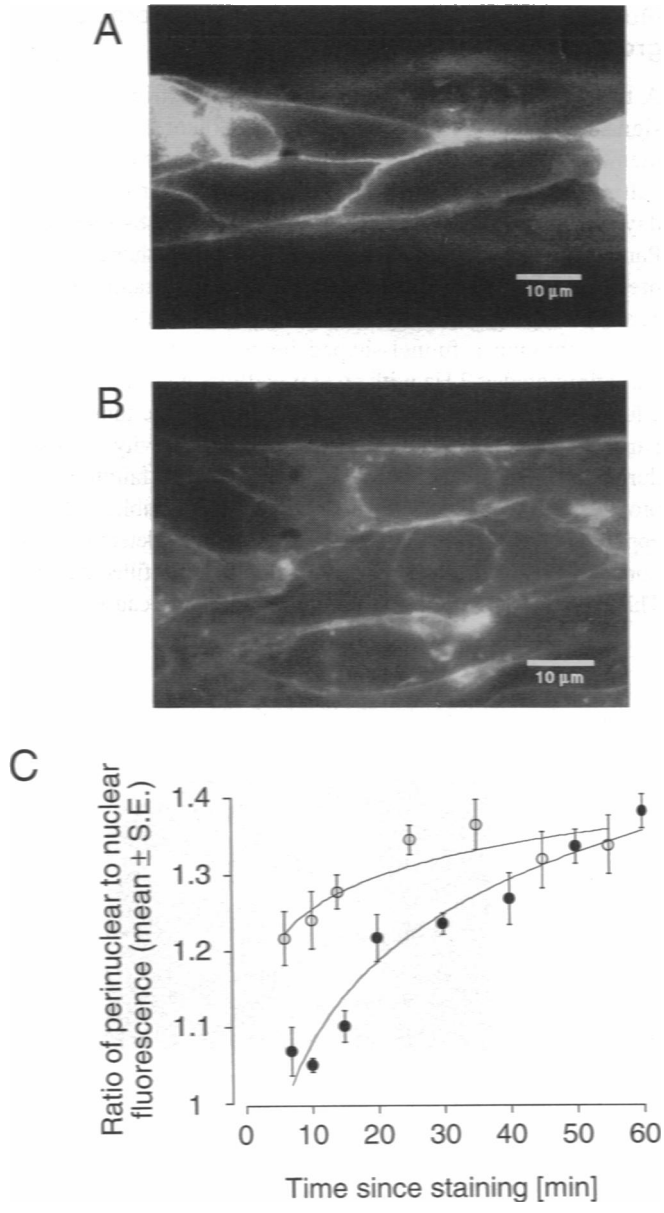

FIGURE 4 Internalization of fluorescent dyes. (*A*) videomicrograph recorded 8 min after staining a patterned growth culture of myocytes with di-8-ANEPPS. (*B*) videomicrograph of the same preparation (different location) taken 38 min after staining. (*C*) Time course of dye internalization for di-4-ANEPPS (○, $n = 8$) and di-8-ANEPPS (●, $n = 8$). Preparations were stained with 20 μg/ml each dye, and the ratio of perinuclear to nuclear fluorescence (ordinate) was monitored during the 60-min period (abscissa) after the end of staining. See text for details.

analogues. In addition, this difference might also account in part for the higher values of the $\Delta F/F$ ratios obtained with di-8-ANEPPS: because the probe molecule stays predominantly in the cell membrane, nonspecific background staining is kept to a minimum, resulting in an increased $\Delta F/F$ ratio compared with those provided by dyes that are more readily internalized. As a result of the findings described, di-8-ANEPPS appeared to be the dye of choice for optical recording of transmembrane voltage in cultured cardiac myocytes.

Multiple site optical recording from patterned growth monolayer cultures

A typical example illustrating the type of extrinsic optical signals provided by multiple site optical recording of transmembrane voltage (MSORTV) in patterned growth myocyte cultures is illustrated in Fig. 5. It was obtained from a three-day-old preparation stained with 80 μg/ml di-8-ANEPPS. Panel *A* is a videomicrograph depicting the shape of the preparation, which consisted of a narrow cell strand (60 μm across) merging gradually with a wide cell strand (3500 μm across) through a funnel-shaped junction. The preparation was stimulated at 2 Hz with an extracellular electrode placed a few millimeters to the left of the image, over the thin strand. Panel *B* depicts the overall pattern of electrical activity recorded during 1 s. The spatial pattern of optical signals faithfully reproduces the geometry of the underlying cell ensemble, with the apparent exception of the signal recorded by a detector positioned in the lower right quadrant marked with a filled square. This signal was recorded from a region that, because it was covered by the photoresist, should have been bare of cells. However, there seemed to be electrically coupled cell-"outliers" on this photoresist part of the pattern, which is consistent with the fluorescent spot, out of focus, at the corresponding location in Panel *A*. The shapes of the action potentials differed among individual recording sites, both with respect to the amplitude of the signal, and the shape of the repolarization phase. Amplitudes tended to be smaller toward the edge of the recording area as a result of a slight fall-off in illumination intensity at the periphery of the field (data not shown). In addition, amplitudes were also smaller along the edges of the funnel and in the row of detectors adjacent to the lower border of the thin cell strand; in both cases, the receptive fields of individual photodiodes were only partially covered with excitable tissue, which explains the uniform reduction in signal amplitude.

Differences among the shapes of the transmembrane signals were confined to the repolarization phase of the action potentials, which were occasionally distorted by the modulation of light scattering by the mechanical contraction that

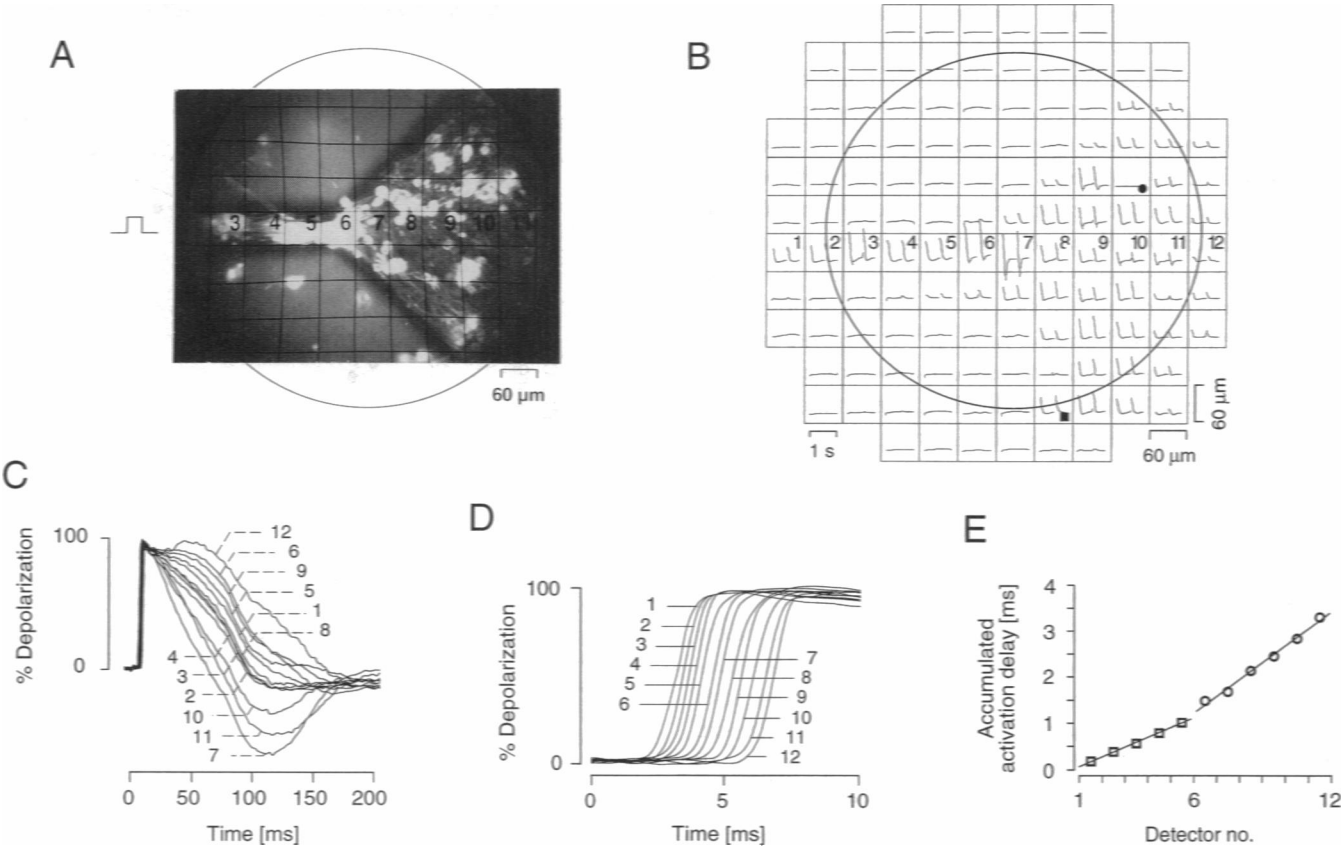

FIGURE 5 Multiple site optical recording of transmembrane voltage (MSORTV) in a patterned growth myocyte monolayer. (*A*) Videomicrograph of preparation with overlaid grid corresponding to the positions of the individual photodetectors. The preparation was stimulated from the left, and each detector monitored a region of the culture measuring 60 μm × 60 μm. (*B*) Signals recorded from all 124 detectors. The round circle corresponds to the circle in *A* and indicates the field of view of the CCD camera, which was slightly smaller than that of the photodiode-array. The numbering of individual detectors corresponds to the numbering in *A*. The recording duration was 1 s; symbols: ■, signals from "aberrant" cells on the photoresist; ●, nonfunctioning detector. (*C*) Illustration of the distortion of the action potential shape by the motion artifact as recorded by the fast data acquisition system in parallel with the recordings shown in *B*. The signals are normalized, and the numbering corresponds to the numbering in *A* and *B*, respectively. (*D*) Expanded view of the upstroke phase of the signals in *C* with corresponding numbering. (*E*) Time of activation recorded by each photodetector as a function of distance (expressed as detector number). The square symbols refer to activation times recorded in the narrow part of the preparation, and the round symbols denote activation times obtained from the detectors that monitor the expanded region of the tissue.

followed activation. Examples of these movement-dependent distortions are depicted in panel *C*. This shows a superposition of the action potentials recorded by the numbered detectors in panels *A* and *B*. Although the upstroke portion of the action potential and the early repolarization phase had an essentially invariant shape, the later phase of repolarization exhibited random distortions. The distortions could be characterized as either positive going (#12) or negative going (#7), but there were also a few records (e.g., #4) that probably represent the timecourse of the action potential with fidelity. In general, action potential shapes with negligible distortions of the repolarization phases were observed routinely from regions of the cultures where monolayers of myocytes were firmly attached to the substrate and where they were free of adhering and intensely stained debris (moribund cells). Although the motion artifacts complicated, and sometimes precluded, the analysis of action potential shapes, the upstroke portions of the transmembrane signals were never contaminated, and the relatively long latency of E-C coupling permitted the determination of activation sequences in the preparations. This is illustrated in panel *D*, which shows the activation sequence along the central row of detectors recorded with the fast data acquisition system. Although individual upstrokes are fast rising and have comparable shapes, activation delays along the preparation are, on average, smaller in the narrow cell strand than in the expanding region. This is illustrated in panel *E*, where the activation times determined along the row of detectors are plotted as a function of distance (expressed as detector number). Both the data obtained in the narrow strand and in the expanding part can be fitted with straight lines ($R = 0.999$ and 0.996, respectively), whose slopes indicate an average conduction velocity of 0.29 m/s in the narrow strand and 0.16 m/s in the funneled region. Similar differences in conduction velocity were observed in all of 9 additional experiments performed on preparations with the same tissue geometry, i.e., a funnel-shaped expansion: although the conduction velocity in the narrow strands was 0.31 ± 0.04 m/s (mean ± SD, $n = 9$; strand width 40–60 μm), it slowed significantly to 0.19 ± 0.03 m/s in the expanding region ($p < 0.0001$; t-test, paired samples; width of the expansion >1500 μm). This decrease in conduction velocity by a factor of 1.6 as the activation wavefront enters the expanding region, which was also observed in growth patterns with different coupling geometries (rectangular, incised; data not shown), could be explained (see Discussion) by a change in the packing arrangement of the cells in the expansion: although the cells were elongated and aligned in the narrow strands, they were oriented at random in the expansion, resulting in an increase in the number of cell-to-cell appositions per unit length, which can hinder impulse propagation in the expanded region.

Concordance between electrical and optical signals

Many investigators working with voltage-sensitive dyes have shown that the timecourse of optically recorded action potentials closely matches the timecourse of the transmembrane action potential as measured by conventional electrophysiological means, and they have found that the fractional fluorescence change is linearly related to the magnitude of the transmembrane voltage change (e.g., Davila et al., 1973; Salzberg et al., 1973; Cohen et al., 1974; Morad and Salama, 1979; Windisch et al., 1985, Chien and Pine, 1991). Generally, it was very difficult to impale the thin cultured myocytes and to maintain a successful impalement during the manipulations necessary to perform a simultaneous optical measurement. However, the few successful experiments showed, without exception, matching action potential shapes for both the electrical and the optical recordings. An example of a recording from a cell in a spontaneously firing cell monolayer is illustrated in panel *A* of Fig. 6. The cell showed a distinct phase-4 depolarization leading to a slowly rising action potential whose repolarization phase was followed by a hyperpolarization. Although the optical recording closely matched the depolarization and the beginning of the repolarizing phase, it deviated from the intracellular recording during the remainder of the repolarization because of the motion artifact. To verify that the fast upward deflection measured optically was indeed an accurate reflection of the action potential upstroke, we compared the time course of the optically measured upstrokes in the presence and absence of the inward sodium current blocker tetrodotoxin (TTX). The amount of TTX used (4 μM) was in the range shown by other investigators to block sodium channels in cultures of neonatal rat heart cells (Robinson and Legato 1980; Cachelin et al., 1983). The results of one such experiment are illustrated in panel *B* of Fig. 6. The preparation was stimulated at 1.4 Hz, and the traces shown correspond to the spatially averaged action potential upstrokes obtained simultaneously from 16 contiguous detectors. The average upstroke velocity of the action potentials recorded under control conditions was 102 ± 10 V/s (mean ± SD), whereas the application of TTX depressed the upstroke velocity to 34 ± 4 V/s (full effect within 5 min). This depressant effect was completely reversible, reaching 95 ± 20 V/s after 15 min of wash-out of the drug. Repetition of this experiment in additional preparations yielded a mean depression of the upstroke velocity to 39% of control during the application of 4 μm TTX, which was significantly different ($p < 0.001$, student t-test) from values obtained during both the control and the washout periods. This rapid and reversible action of TTX on the velocity of the action potential upstroke demonstrates that the fast initial deflection of the optical recording corresponds to the action potential upstroke, and also shows that these cultured myocytes have functional sodium channels.

Signal transfer between myocytes and nonmyocytes

Despite the elaborate preplating procedure (c.f. Materials and Methods), cardiac myocyte cultures contained a small number of noncontracting cells that are presumably nonexcitable and that could be assigned, based on their shape, to two

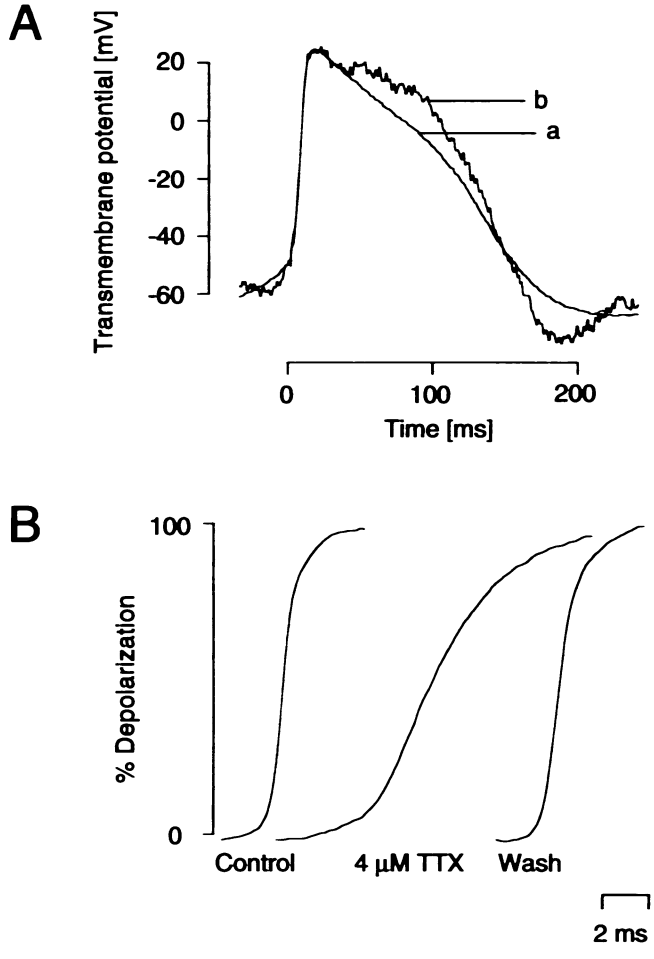

FIGURE 6 Microelectrode recordings of transmembrane voltage compared with optical recordings, and the effect of TTX on the optically recorded action potential upstroke. (*A*) Superposition of an action potential recorded with an intracellular electrode (a) and of the scaled optical signal of the same event recorded simultaneously (b). (*B*) The three curves shown represent the spatial averages of 16 optical signals recorded simultaneously by contiguous detectors, obtained under control conditions (*left*), during the application of 4 μm TTX (*middle*), and after wash-out of the drug (*right*). The amplitudes are normalized and the time calibration applies to all traces.

groups. One group, the fibroblasts, consisted of randomly interspersed solitary large cells (roughly 2–3 times the area of myocytes) having irregularly pointed shapes and a thin translucent cell body devoid of coarse granulations and myofibrils. The cells of the second group always occurred in clusters forming a tight monolayer with "cobblestone" morphology and bear a close resemblance to an epithelium, particularly because of the uniform polygonal shape of individual cells. Because the origin of the second group was either the endothelium of the endocardium/cardiac vasculature or the mesothelial cells of the pericardium, both of which were also trypsinized during the culturing procedure, we have termed them endotheloid cells. A recent report described cells of exactly the same morphology as being of epicardial mesothelial origin (Eid et al., 1992) based on immunohistochemical and ultrastructural evidence. Because we made no further efforts to identify these cells exactly, we retain the description "endotheloid" throughout this paper. Both cell types always occurred in close contact with the myocytes and, therefore, we were interested in whether they were also electrically coupled to the myocytes.

An example of a large fibroblast contacting a strand of myocytes is illustrated in Fig. 7. Electrical activity as shown in panel *B* is clearly restricted to the region of the preparation containing cells, and triangularly shaped signals can be seen over the region covered by the fibroblast, corroborating earlier findings of electrical coupling between myocytes and fibroblasts in culture (Hyde et al., 1969; Jongsma et al., 1989). The small negative deflection recorded two sites up from detector 1 (and by the adjacent pixel) occurs at the same time as the motion artifact recorded by the element below and is likewise an isolated motion artifact. Panel *C* shows the superposition of normalized action potential upstrokes recorded from myocytes (pixels 1 and 2) from myocytes in contact with the fibroblast (pixels 3–5) and from the fibroblast itself (pixels 6–9). The potentials recorded from the fibroblast have a distinctly slower rise time than those recorded from the myocytes on the left, whereas the myocytes in contact with the fibroblast show intermediate values, suggesting electrical coupling between the fibroblast and the myocytes, where the inexcitable fibroblast imposes an electrical load on adjacent myocytes, slowing their upstrokes.

Electrical coupling between myocytes and the second type of nonmyocyte cells, the endotheloid cells, is illustrated in Fig. 8. The preparation consisted of a linear strand of myocytes lying on top of a short patch of endotheloid cells forming a tight cell monolayer. In the center of the field, the continuity of the myocyte strand was maintained only by a single cell (pixels 6–8). Although some of the signals from the two central rows shown in panel *B* (e.g., pixels 6–8 corresponding to the myocyte strand) show typical distortions of the repolarization phase resulting from motion artifacts, all of the signals originating in the adjacent, pure endotheloid cell layer exhibited potential changes characteristic of action potentials, but free from any contaminating contraction artifacts. Again, as in the case of the fibroblast, this suggests the presence of electrical coupling between myocytes and endotheloid cells in culture. Panel *C* shows the upstroke portions of the signals recorded from the numbered row of detectors, which monitor both the endotheloid cell layer and the overlaid myocyte strand at high temporal resolution. Impulse propagation is clearly delayed as the action potential reaches the constricted region. Although the leftmost detector exhibits a nearly normal upstroke shape, with a negligible secondary depolarizing hump, downstream regions show progressively depressed upstroke amplitude and velocity, followed by a steadily increasing secondary depolarization. This secondary depolarization coincides in time with the upstroke recorded by the detectors on the right. These latter upstrokes arise from a pronounced prepotential and are delayed, compared with the upstrokes recorded on the left, by approximately 3 ms, resulting in an apparent overall velocity of 0.02 m/s. Whether this delay resulted from the coupling of the endotheloid cells (presumably nonexcitable) to the

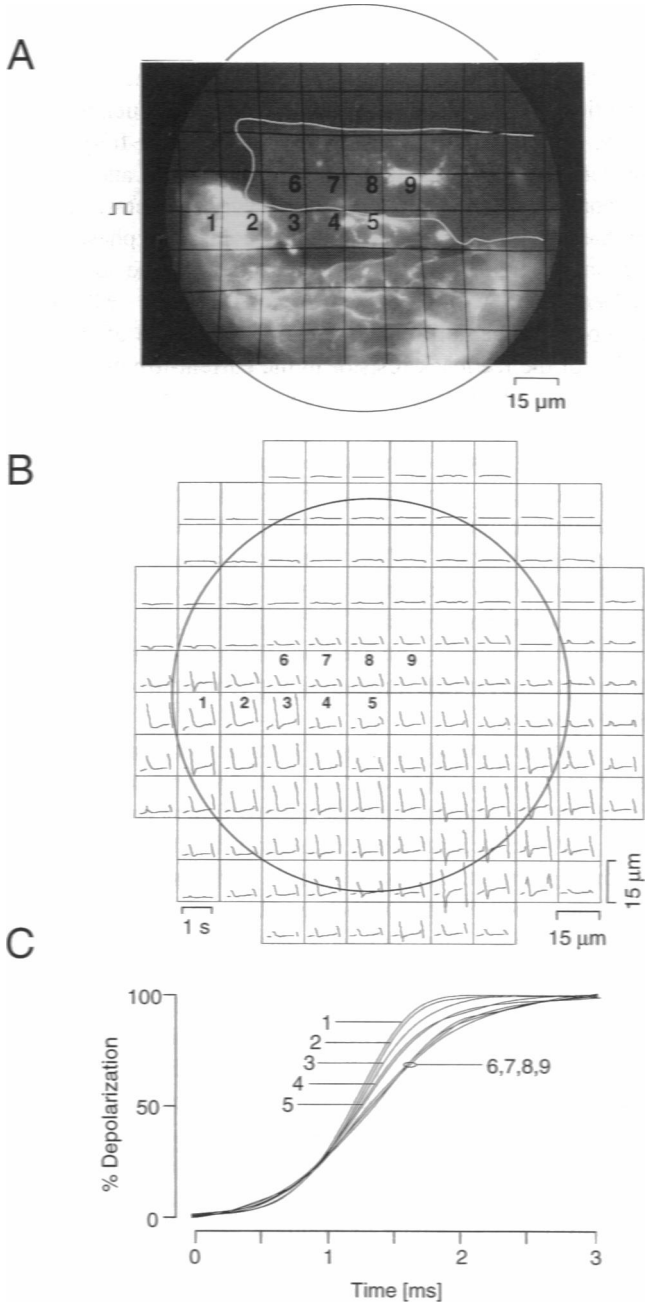

FIGURE 7 Electrical coupling between a fibroblast and a monolayer strand of ventricular myocytes. (*A*) Videomicrograph of the preparation with an overlaid grid corresponding to the positions of individual photodetectors. The preparation was stimulated from the left, and each detector monitored electrical activity from a region measuring 15 μm × 15 μm. The white line corresponds to the (partial) outline of the fibroblast. (*B*) Signals recorded from all 124 detectors during a 1-s interval. The round circle corresponds to the circle in *A*, indicating the field of view of the video camera with respect to the photodiode array. The numbering of the individual detectors corresponds to the numbering in *A*. (*C*) Action potential upstrokes recorded by detectors imaging the fibroblast (numbers 6–9) and the neighboring myocytes; corresponding numbering.

small myocyte layer, with the increased electrical load compromising impulse propagation, or whether the delay was caused by the geometry of the myocyte strand itself (Rohr and Salzberg, 1994) with its pronounced local thinning remains speculative.

DISCUSSION

The successful implementation of the optical recording technique for the purpose of measuring action potential propagation, with microsecond time resolution, on a cellular/subcellular scale depended on the following prerequisites. (i) Signal-to-noise ratios had to be large enough to identify unambiguously fiducial points from which activation delays as small as 30 μs (detector-to-detector delay at a conduction velocity of 0.5 m/s viewed with a X100 objective) could be measured. (ii) Photodiode-amplifier combinations were required to exhibit sufficient uniformity and synchronicity to permit the determination of activation delays with microsecond time resolution. (iii) Phototoxicity of the potentiometric probes needed to be minimized to avoid unwanted secondary effects on propagation. (iv) The positions of the individual detectors with respect to the images of the preparations had to be determined with sufficient precision to permit the derivation of structure-function-relationships. (v) Depending on the experimental aims, individual myocytes contributing to propagation had to be identifiable. The last two points are not discussed further because one of the hallmarks of monolayer cell cultures is the ease with which individual cells can be identified, and the MSORTV system described in Materials and Methods section, permitted the unambiguous determination of the location of the receptive fields of individual photodiodes in the cell layer.

The signal-to-noise ratio is, in the photon noise-limited case, directly proportional to the maximal fluorescence change for a given transmembrane voltage change and is inversely proportional to the square root of the resting fluorescence intensity. Therefore, we screened a wide variety of voltage-sensitive dyes to find the probe having the highest $\Delta F/F$ ratio. Di-8-ANEPPS gave the largest signals (average $\Delta F/F$ with narrow excitation filter around 15% per 100 mV), and was used routinely in most of our experiments. Because our measurements were always detector noise-limited, an increase in illumination intensity (and resting fluorescence) should have been accompanied by a proportional increase in the signal-to-noise ratio. Therefore, we increased the incident illumination intensity by choosing wide bandwidth excitation filters and by replacing our original 250 W tungsten halogen lamp with a 150 W xenon short arc lamp. Using this approach, signal-to-noise ratios (peak-to-peak) were increased to values (25–40) suitable for resolving action potential upstrokes during single trial experiments, so that unambiguous determination of activation delays was possible. Although numerous investigators have shown that optically and electrically recorded action potentials are identical in shape (Salzberg et al., 1973; Cohen et al., 1974; Salzberg et al., 1977; Morad and Salama, 1979, Windisch et al., 1985), we showed that the fast upstrokes measured optically in our system depended upon the activation of voltage-sensitive sodium channels, as evidenced by their reversible depression during application of blocking amounts of TTX (cf. Salzberg et al., 1983).

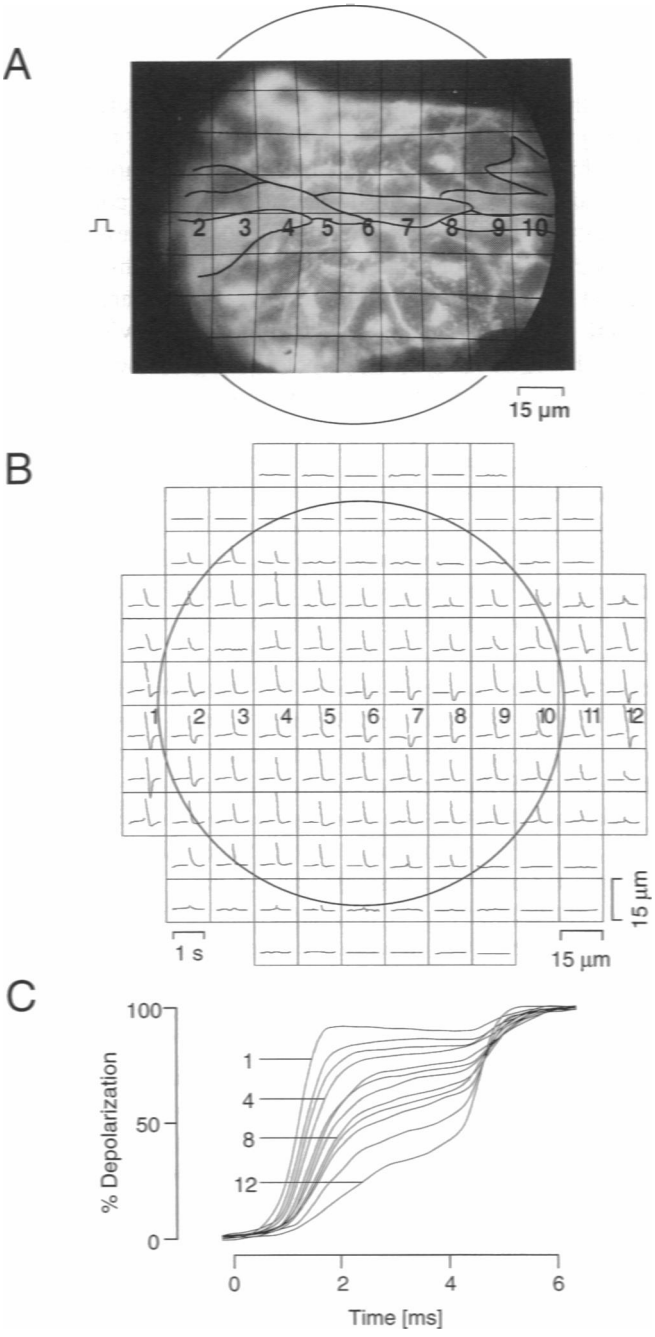

FIGURE 8 Electrical coupling between endotheloid cells and a monolayer strand of ventricular myocytes. (*A*) Videomicrograph of the preparation with an overlaid grid corresponding to the positions of individual photodetectors. The preparation was stimulated from the left and each detector monitored electrical activity from a region measuring 15 μm × 15 μm. The black lines correspond to the outlines of individual myocytes forming a thin strand on top of the endothelial layer. (*B*) Signals recorded from all 124 detectors during a 1-s interval. The round circle corresponds to the circle in *A*, indicating the field of view of the video camera with respect to the photodiode array. The numbering of individual detectors corresponds to the numbering in *A*. (*C*) Action potential upstrokes recorded by the central row of detectors imaging the myocytes, together with the underlying endotheloid cells; corresponding numbering.

An optimal system for the determination of action potential propagation on a microscopic scale would consist of detector-amplifier combinations having high, and absolutely identical, frequency responses. The cutoff frequency needs to be high compared with that of the maximal frequencies present in the biological preparation of interest, and the corresponding data conversion system needs to operate at a rate high enough to resolve accurately the upstroke phase of the action potential. Our system deviated from the ideal with respect to the frequency response of the MSORTV photodetector-amplifier combinations: because of the high value of the feedback resistor in the current-to-voltage converter (10^9 Ohm), time constants ranged between 150 and 200 μs and, therefore, were slow compared with the rise times achieved with compensated intracellular electrode amplifiers (20 μs, Barr and Spach, 1977). However, the two remaining requirements, i.e., identical frequency responses among the detectors and high data acquisition rates could be implemented. We achieved an optical response time homogeneity among all detectors of ± 5 μs using the procedures outlined in Materials and Method. This precision allowed us to monitor accurately propagation phenomena on a microscopic scale.

A significant disadvantage of optical recording, the presence of phototoxic effects tied to the generation of singlet oxygen by the excited state of the probe molecules (Oxford et al., 1977; Salzberg, 1983), was carefully studied to restrict recording times to an initial interval free of such effects. We used the time constant of the fast phase of the decay of the action potential amplitude as a parameter to quantitate the severity of photodynamic damage and found that the dye that exhibited the highest fractional fluorescence change (di-8-ANEPPS) also had the slowest decay of the signal amplitude. This dye provided a window of up to 10 s, during which the minimal decay in amplitude could be fully explained by the dye's bleaching. Decay rates significantly in excess of the bleaching rate occurred only after this time interval. In contrast, the closely related dye, di-4-ANEPPS, which differed from di-8-ANEPPS only in having a 50% shorter hydrocarbon chain length, exhibited major phototoxic effects from the very start of illumination with comparable intensities. Puzzled by this observation, and supposing that the longer hydrocarbon chain length should enhance the retention of the dye in the membrane (Fluhler et al., 1985), we tried to examine how the two dyes were internalized. We had previously noticed that the cell interior of myocytes stained with di-4-ANEPPS turned fluorescent very shortly after the staining process. The most prominent feature of this internal staining was the appearance of a bright halo around the nucleus, consisting most probably of local accumulations of stained cytoplasmic membranes (Golgi, SR). The development of a similar halo was also observed in the case of di-8-ANEPPS; however, it appeared at a much slower rate. Because significant probe internalization depending upon a flip-flop process across the membrane can be excluded by the presence of an hydrophilic sulfonate group occurring at identical positions in both dyes, internalization should be considered in

the context of endocytotic membrane cycling (Silverstein et al., 1977). We can speculate that, given equal levels of endocytotic membrane cycling, the dye with the lower membrane binding constant (di-4-ANEPPS) would be more prone to depart the endocytotic vesicle after fusion with other intracellular cell organelles. Di-8-ANEPPS, on the other hand, would have an increased tendency to stay in the membrane and become reintegrated into the cell membrane during the process of "membrane shuttling" between these intracellular organelles and the sarcolemma. The difference in the rate of internalization and the difference in photodynamic potency between these two very similar dyes could possibly be rationalized by the suggestion that the free radicals, including singlet oxygen, having the most deleterious effects are those generated in the cell interior, whereas those arising in or near the cell membrane exhibit a delay of several seconds before the onset of phototoxicity.

With our system for MSORTV, we have been able to observe the patterns of electrical activity in both normal monolayer cultures of neonatal rat heart cells and in cultures where the growth of cells has been patterned to study the dependence of impulse propagation on the cellular architecture of the underlying excitable tissue. Experiments with myocyte patterns consisting of narrow cell strands merging abruptly with wide tissue expansions revealed that impulse propagation velocity was 1.6 times faster in the narrow strands than in the expanded regions. Because differences in active membrane properties can be ruled out as the cause for this finding (homogeneous cell population), it is likely that the difference results from the passive properties of the cellular network, similar to the anisotropic conduction found in the intact heart (Clerc, 1976). A likely morphological substrate for the differing passive properties in the two regions is the consistent finding that cells in narrow growth channels were elongated and aligned, whereas those in expanded regions were slightly more rounded and randomly aligned. From previously published morphological data on patterned growth cultures (Rohr et al., 1991), it can be calculated that, on average, cell-to-cell boundaries in narrow channels with elongated and aligned cells occur every 52 μm, whereas in expanded regions (monolayers) these boundaries occur 21 μm apart (mean cytoplasmic distances within rectangular cells measuring 55 μm $\times$ 16 μm, which are aligned at random with respect to the direction of propagation of the action potential). Based on (i) these cell-to-cell distances; (ii) the assumption that conduction velocity *within* a cell is independent of the direction of the propagating impulse; (iii) the finding that gap junctions are uniformly distributed along the cell boundaries (results from immunohistochemical stainings for connexin 43 in these cultures; data not shown); and (iv) the differences in conduction velocity in the thin (0.31 m/s) vs. the wide (0.19 m/s) region of the preparation, we calculate that the activation wavefront is delayed by approximately 70 μs at the cell-to-cell boundaries. This value, which suggests discontinuous impulse propagation at the level of single myocytes, is slightly lower than previous direct determinations of junctional delays in chains of single myocytes (Rohr and Salzberg, 1992b; Fast and Kleber, 1993). This difference can be explained by the circumstance that the homogeneous distribution of gap junctions along the cell boundaries offers the depolarizing current a collateral path through neighboring cells, thereby decreasing the effect of the recurrent augmentations in longitudinal (junctional) resistance.

We sometimes observed that two types of noncontracting and presumably nonexcitable cells, fibroblasts and endotheloid cells, grew in close contact with myocytes in our cultures (Rohr et al., 1991). Earlier attempts to impale these cells with microelectrodes had failed because of the thinness of the cells and because their membranes are very fragile. Optical recording now offered the possibility of studying whether these cells were electrically coupled to the myocytes. The optical signals recorded from fibroblasts were identical to those recorded from myocytes, except for their slower upstroke velocity and the absence of a motion artifact. These findings are in agreement with earlier descriptions of electrical coupling between these two cell types (Hyde et al., 1969; Jongsma et al., 1989) and the reduced upstroke velocity exhibited by the myocytes with increasing proximity to the fibroblast illustrates the electrical load imposed by the fibroblast on the active cells. With respect to the second cell type, the endotheloid cells, a recent report (Eid et al., 1992) described the existence of dye coupling (lucifer yellow) between cells of exactly the same morphology (identified as being of epicardial-mesothelial origin) and apposed myocytes in a culture system. Our results demonstrate that, in addition, these cells are well coupled among themselves electrically, and coupled also to the cardiac myocytes. The shapes of the optical signals recorded from these cells were also similar to those of action potentials normally recorded from myocytes, with the exception that, once again, no signs of motion artifact were present. In the example presented, impulse propagation recorded from a thin strand of myocytes lying on top of the cobblestone-like cell layer was delayed by several milliseconds while crossing the patch of endotheloid cells. Because of the electrical coupling between the two types of cells, it can be argued that the electrotonic load represented by the passive endotheloid cells on the thin strand of myocytes critically drained the activation current that would otherwise have contributed to excitation downstream, thereby giving rise to the large delay. The slowing of propagation, however, could also have resulted directly from the extreme narrowing of the myocyte strand, as is shown in a different paper (Rohr and Salzberg, 1994).

In conclusion, we have been able to record low noise optical signals, representing electrical activity, from cultures of neonatal rat heart cells at high spatial and temporal resolution. The signal-to-noise ratio is sufficient to determine activation delays between adjacent regions of the tissue separated by 15 μm, without averaging, using a di-octyl styryl dye. This molecular voltmeter proved to be a suitable indicator in terms both of fractional fluorescence change per unit change in membrane potential and of decreased propensity for causing photodynamic damage. Using this system, we could show that ventricular myocytes were electrically

coupled to both fibroblasts and endotheloid cells, which were sporadically present in the cultures. The optically measured spatial and temporal characteristics of propagating action potentials revealed that, as in the intact heart, conduction velocity depends upon the micro-architecture of the tissue; the results obtained from morphological and functional comparisons between narrow and wide cell strands support the model of discontinuous propagation at the level of single myocytes.

We are grateful to Ana Lia Obaid, Larry Cohen, and Sanjay Kumar for helpful discussions, and we are deeply indebted to Leslie Loew, Amiram Grinvald, and Rina Hildesheim for providing us with numerous dyes.
This work was supported by the Swiss National Science Foundation grant 823A-028424 and a fellowship from the Grass Foundation to S. Rohr and U.S. Public Health Service grant NS16824 to B. M. Salzberg.

REFERENCES

Barr, R. C., and M. S. Spach. 1977. Sampling rates required for digital recording of intracellular and extracellular cardiac potentials. *Circulation.* 55:40–48.

Brugada, J., L. Boersma, C. J. H. Kirchhof, V. V. Th. Heynen, and M. A. Allessie. 1991. Reentrant excitation around a fixed obstacle in uniform anisotropic ventricular myocardium. *Circ. Res.* 84:1296–1306.

Cachelin, A. B., J. E. De Peyer, S. Kokobun, and H. Reuter. 1983. Sodium channels in cultured cardiac cells. *J. Physiol.* 340:389–401.

Chien, C. B., and J. Pine. 1991. Voltage-sensitive dye recording of action potentials and synaptic potentials from sympathetic microcultures. *Biophys. J.* 60:697–711.

Clerc, L. 1976. Directional differences of impulse spread in trabecular muscle from mammalian heart. *J. Physiol.* 255:335–346.

Cohen, L. B., and B. M. Salzberg. 1978. Optical measurement of membrane potential. *In* Reviews of Physiology, Biochemistry, and Pharmacology. Springer-Verlag, New York. 83:33–88.

Cohen, L. B., B. M. Salzberg, H. V. Davila, W. N. Ross, D. Landowne, A. S. Waggoner, and C.-H. Wang. 1974. Changes in axon fluorescence during activity: molecular probes of membrane potential. *J. Membr. Biol.* 19:1–36.

Dillon, S., and M. Morad. 1981. A new laser scanning system for measuring action potential propagation in the heart. *Science.* 214:453–455.

Durrer, D., R. Th. Van Dam, G. E. Freud, M. J. Janse, F. L. Meijler, and R. C. Arzbaecher. 1970. Total excitation of the isolated human heart. *Circulation.* 41:899–912.

Eid, H., D. M. Larson, J. P. Springhorn, M. A. Attawia, R. C. Nayak, T. W. Smith, and R. A. Kelly. 1992. Role of epicardial mesothelial cells in the modification of phenotype and function of adult rat ventricular myocytes in primary coculture. *Circ. Res.* 71:40–50.

Fast, V. G., and A. G. Kleber. 1993. Microscopic conduction in cultured strands of neonatal rat heart cells measured with voltage-sensitive dyes. *Circ. Res.* 73:914–925.

Fluhler, E., V. G. Burnham, and L. M. Loew. 1985. Spectra, membrane binding, and potentiometric responses of new charge shift probes. *Biochemistry.* 24:5749–5755.

Grinvald, A., D. Frostig, E. Lieke, and R. Hildesheim. 1988. Optical imaging of neuronal activity. *Physiol. Rev.* 68:1285–1366.

Grinvald, A., R. Hildesheim, I. C. Farber, and L. Anglister. 1982. Improved fluorescent probes for the measurement of rapid changes in membrane potential. *Biophys. J.* 39:301–308.

Grinvald, A., R. Hildesheim, R. Gupta, and L. B. Cohen. 1980. Better fluorescent probes for optical measurement of membrane potential. *Biol. Bull. Mar. Biol. Lab.* 159:484.

Henriquez, C. S., and R. Plonsey. 1987. Effects of resistive discontinuities on waveshape and velocity in a single cardiac fibre. *Med. Biol. Eng. Comp.* 25:428–438.

Hyde, A., B. Blondel, A. Matter, J. P. Cheneval, B. Filloux, and L. Girardier. 1969. Homo- and heterocellular junctions in cell cultures: an electrophysiological and morphological study. *Prog. Brain Res.* 31:283–311.

Israel, D. A., D. J. Edell, and R. G. Mark. 1990. Time delays in propagation of cardiac action potential. *Am. J. Physiol.* 258:H1906–H1917.

Jongsma, H. J., M. B. Rook, A. C. C. van Ginneken, and B. de Jonge. 1989. Homo- and heterotypic gap junctions between cardiac myoblasts and fibroblasts: difference in single channel properties. *Biophys. J.* 55:218*a*. (Abstr.)

Jongsma, H. J., and H. E. van Rijn. 1972. Electrotonic spread of current in monolayer cultures of neonatal rat heart cells. *J. Membr. Biol.* 9:341–360.

Kamino, K. 1991. Optical approaches to ontogeny of electrical activity and related functional organization during early heart development. *Physiol. Rev.* 71:53–91.

Kamino, K., A. Hirota, and S. Fujii. 1981. Localization of pacemaking activity in early embryonic hearts monitored using a voltage sensitive dye. *Nature.* 290:595–597.

Lewis, T., J. Meakins, and P. D. White. 1914. The site of origin of the mammalian heartbeat: the pacemaker in the dog. *Heart.* 2:147–169.

Loew, L. M., L. B. Cohen, J. Dix, E. N. Fluhler, V. Montana, G. Salama, and J. Y. Wu. 1992. A naphthyl analog of the aminostyryl pyridinium class of potentiometric membrane dyes shows consistent sensitivity in a variety of tissue, cell, and model membrane preparations. *J. Membr. Biol.* 130:1–10.

Morad, M., and G. Salama. 1979. Optical probes of membrane potential in heart muscle. *J. Physiol.* 292:267–295.

Murphey, C. R., J. W. Clark, W. R. Giles, R. L. Rasmusson, J. A. Halter, K. Hicks, and B. Hoyt. 1991a. Conduction in bullfrog atrial strands: simulations of the role of disc and extracellular resistance. *Math. Biosci.* 106:39–84.

Murphey, C. R., J. W. Clark, and W. R. Giles. 1991b. A model of slow conduction in bullfrog atrial trabeculae. *Math. Biosci.* 106:85–109.

Oxford, G. S., J. P. Pooler, and T. Narahashi. 1977. Internal and external application of photodynamic sensitizers on squid giant axons. *J. Membr. Biol.* 36:159–173.

Parsons, T. D., B. M. Salzberg, A. L. Obaid, F. Raccuia-Behling, and D. Kleinfeld. 1991. Long-term optical recording of patterns of electrical activity in ensembles of cultured Aplysia neurons. *J. Neurophysiol.* 66: 316–333.

Pertsov, A. M., J. M. Davidenko, R. Salomonsz, W. T. Baxter, and J. Jalife. 1993. Spiral waves of excitation underlie reentrant activity in isolated cardiac muscle. *Circ. Res.* 72:631–650.

Pollard, A. E., M. J. Burgess, and K. W. Spitzer. 1993. Computer simulation of three-dimensional propagation in ventricular myocardium: effects of intramural fiber rotation and inhomogeneous conductivity on epicardial activation. *Circ. Res.* 72:744–756.

Robinson, R. B., and M. J. Legato. 1980. Maintained differentiation in rat cardiac monolayer cultures: tetrodotoxin sensitivity and ultrastructure. *J. Mol. Cell. Cardiol.* 12:493–498.

Rohr, S. 1986. Temperature-controlled perfusion chamber suited for mounting in microscope stages. *J. Physiol.* 378:90*a*. (Abstr.)

Rohr, S., and B. M. Salzberg. 1992a. Multiple site optical recording of transmembrane voltage from cultures of rat ventricular myocytes. *Biophys. J.* 61:2555*a*. (Abstr.)

Rohr, S., and B. M. Salzberg. 1992b. Discontinuities in action potential propagation along chains of single ventricular myocytes in culture: multiple site optical recording of transmembrane voltage (MSORTV) suggests propagation delays at the junctional sites between cells. *Biol. Bull. Mar. Biol. Lab.* 183:342–343.

Rohr, S., and B. M. Salzberg. 1994. Characterization of impulse propagation at the microscopic level across geometrically defined expansions of excitable tissue: multiple site optical recording of transmembrane voltage (MSORTV) in patterned growth heart cell cultures. *J. Gen. Physiol.* 104: 287–309.

Rohr, S., D. M. Schölly, and A. G. Kleber. 1991. Patterned growth of neonatal rat heart cells in culture: morphological and electrophysiological characterization. *Circ. Res.* 68:114–130.

Rosenbaum, D. S., D. T. Kaplan, A. Kanai, L. Jackson, H. Garan, R. J. Cohen, and G. Salama. 1991. Repolarization inhomogeneities in ventricular myocardium change dynamically with abrupt cycle length shortening. *Circ.* 84:1333–1345.

Ross, W. N., B. M. Salzberg, L. B. Cohen, A. Grinvald, H. V. Davila, A. S. Waggoner, and C.-H. Wang. 1977. Changes in absorption, fluorescence, dichroism, and birefringence in stained giant axons: optical measurement of membrane potential. *J. Membr. Biol.* 33:141–183.

Rudy, Y., and W. Quan. 1987. A model study of the effects of the discrete cellular structure on electrical propagation in cardiac tissue. *Circ. Res.* 61:815–823.

Rudy, Y., and W. Quan. 1991. Propagation delays across cardiac gap junctions and their reflection in extracellular potentials: a simulation study. *J. Cardiovasc. Electrophysiol.* 2:299–315.

Salama, G., and M. Morad. 1976. Merocyanine 540 as an optical probe of transmembrane electrical activity in the heart. *Science.* 191:485–487.

Salzberg, B. M. 1983. Optical recording of electrical activity in neurons using molecular probes. *In* Current Methods in Cellular Neurobiology. J. L. Barker and J. E. McKelvy, editors. John Wiley & Sons, New York. 139–187

Salzberg, B. M. 1989. Optical recording of voltage changes in nerve terminals and in fine neuronal processes. *Annu. Rev. Physiol.* 51:507–526.

Salzberg, B. M., H. V. Davila, and L. B. Cohen. 1973. Optical recording of impulses in individual neurons of an invertebrate central nervous system. *Nature.* 246:509–509.

Salzberg, B. M., A. Grinvald, L. B. Cohen, H. V. Davila, and W. N. Ross. 1977. Optical recording of neuronal activity in an invertebrate central nervous system: Simultaneous monitoring of several neurons. *J. Neurophysiol.* 40:1281–1291.

Salzberg, B. M., A. L. Obaid, D. M. Senseman, and H. Gainer. 1983. Optical recording of action potentials from vertebrate nerve terminals using potentiometric probes provides evidence for sodium and calcium components. *Nature.* 306:36–40.

Sawanobori, T., A. Hirota, S. Fujii, and K. Kamino. 1981. Optical recording of conducted action potential in heart muscle using a voltage-sensitive dye. *Japan J. Physiol.* 31:369–380.

Shumaker, J. M., J. W. Clark, and W. R. Giles. 1993. Simulations of passive properties and action potential conduction in an idealized bullfrog atrial trabeculum. *Math. Biosci.* 116:127–167.

Silverstein, S. C., R. M. Steinman, and Z. A. Cohn. 1977. Endocytosis. *Annu. Rev. Biochem.* 46:669–722.

Spach, M. S., E. R. Darken, and K. H. Raines. 1990. A method of microscopic mapping of cardiac excitation spread. *Ann. Int. Conf. IEEE Eng. Med. Biol. Soc.* 12:591–592.

Spach, M. S., and J. M. Kootsey. 1983. The nature of electrical propagation in cardiac muscle. *Am. J. Physiol.* 244:H3–H22.

Spach, M. S., W. T. Miller III, D. B. Geselowitz, R. G. Barr, J. M. Kootsey, and E. A. Johnson. 1981. The discontinuous nature of propagation in normal canine cardiac muscle. Evidence for recurrent discontinuities of intracellular resistance that affect the membrane currents. *Circ. Res.* 48: 39–54.

Ursell, P. C., P. I. Gardner, A. Albala, J. J. Fenoglio, Jr., and A. L. Wit. 1985. Structural and electrophysiological changes in the epicardial border zone of canine myocardial infarcts during infarct healing. *Circ. Res.* 56: 436–451.

Waggoner, A. S., and A. Grinvald. 1977. Mechanism of fast optical changes of potential sensitive dyes. *Ann. N. Y. Acad. Sci.* 303:217–242.

Windisch, H., W. Müller, and H. A. Tritthart. 1985. Fluorescence monitoring of rapid changes in membrane potential in heart muscle. *Biophys. J.* 48:877–884.

Wit, A. L., M. A. Allessie, F. I. M. Bonke, W. Lammers, J. Smeet, and J. J. Fenoglio, Jr. 1982. Electrophysiologic mapping to determine the mechanism of experimental ventricular tachycardia initiated by premature impulses. *Am. J. Cardiol.* 49:166–185.

Witkowski, F. X., R. Plonsey, P. A. Penkoske, and K. M. Kavanagh. 1994. Significance of inwardly directed transmembrane current in determination of local myocardial electrical activation during ventricular fibrillation. *Circ. Res.* 74:507–524.